A 4D Imaging Tool for Lagrangian Particle Tracking in Stirred Tanks

Y. Cheng and F. J. Diez
Dept. of Mechanical and Aerospace Engineering, Rutgers, The State University of New Jersey, Piscataway, NJ 08854

DOI 10.1002/aic.12429
Published online October 11, 2010 in Wiley Online Library (wileyonlinelibrary.com).

A time-resolved volumetric 3D particle tracking tool is presented for mixing in stirred tanks studies and its capabilities are explored in a low Reynolds number custom-made stirred tank. The technique provides a Lagrangian description of particles in the flow resolving their 3D trajectories, velocities, and acceleration. The optimization of the system allowed, for the first time, tracking ~400 particles at a time in an imaged volume (60 mm × 60 mm × 50 mm) in the stirred tank. The system was validated in a 1-D piston-driven flow and by comparing the measurements with a 2D-particle image velocimetry system in a stirred tank. Results show the advantages of this technique to understand particle dynamics. Sample measurements illustrated that small changes in the stirrer configuration produced an unexpected variety of particle trajectories which were classified according to their path shape and location. Particle velocities and Lagrangian accelerations provided new insights into their mixing process. © 2010 American Institute of Chemical Engineers *AIChE J,* 57: 1983–1996, 2011
Keywords: mixing, fluid mechanics, particulate flows, particle/count/measurements

Introduction

Stirred tanks are widely used in the mixing and blending of particulate materials including pharmaceutical ingredients, chemicals, or food processing ingredients among others. But while low Reynolds numbers mixing in stirred tanks is of interest to the community[1] its flow behavior is not well understood, and it tends to have lower efficiency and side reaction effects. This is in part due to the lack of knowledge about the dynamics of the constituents (i.e., fluid and particles) which need to be time resolved. The most established tool to study mixing in stirred tanks has been by means of computational simulations. This includes the use of traditional computational fluid dynamics (CFD)[2–7] and discrete element methods (DEM) to incorporate liquid-solid systems, CFD-DEM.[8] Although numerical methods can provide 2D and 3D flow results, validations are still needed through experimental methods.

Correspondence concerning this article should be addressed to F. J. Diez at diez@jove.rutgers.edu.

Experimental measurements in stirred tanks have been performed by many researchers. Many involve optical flow measurement techniques such as phase Doppler velocimetry (PDV), particle image velocimetry (PIV), and planar laser induce fluorescence (PLIF), among others. These are nonintrusive methods with, in general, higher spatial and temporal resolution than nonoptical techniques and commonly used to visualize the flow and to provide velocity or concentration measurements (instantaneous and average values). For example, Guiraud et al.[9] applied the phase Doppler technique to study turbulent mixing in a fully baffled vessel with an industrial axial propeller and obtained 2D velocity fields near the stirrer. Similarly, a phase-locked stereoscopic PIV system was applied on three different vertical planes close to the impeller of a stirred tank to get 2D velocity fields.[10] Also Lamberto et al.[11] used fluorescent dye and a 2D-PIV system to investigate, together with CFD simulations, the flow in an unbaffled stirred tank. Their study shows the dominant flow structures in the stirred tank, but fails to provide quantitative particle trajectory information to understand the dynamics of the mixing process. These and similar optical techniques[12–15]

provide an Eulerian description of the flow in stirred tanks. Nevertheless, it would be desirable to obtain a Lagrangian description of particle trajectories which would provide a better understanding of the dynamics of the mixing process. A Lagrangian experimental approach would also allow better comparison to numerical results such as those from CFD calculations.

To obtain particle trajectories and a Lagrangian description of the flow, nonoptical techniques are commonly used. For instance, particle trajectories can be obtained by using positron emission particle tracking (PEPT).[16] The measurements were made in a stirred vessel with axial impellers. However, the system requires costly equipments like positron cameras and position-sensitive gamma-ray detector. Another technique known as computer automated radioactive particle tracking (CARPT) was used to study the solid suspension in a stirred tank reactor[17] and particle motion in packed/ebullated beds.[18] The CARPT system maps the motion of the solids by tracking single radioactive particles that are of same size and density as the actual solids. This is one of the few techniques available when optical access to the flow is not possible but the system requires a delicate calibration procedure and is of considerable complexity. Also, neither the PEPT nor the CARPT technique can produce more than a few particle trajectories at a time which does not give a full description of the dynamics of the flow.

The approach presented requires optical access to the flow, and it describes a time resolved volumetric measurement technique capable of individually and simultaneously tracking up to ~400 particles in a stirred tank to provide their Lagrangian trajectories. This technique, known as three-dimensional particle tracking velocimetry (3D-PTV) has been recently introduced in other fields of research for its comprehensive flow measurement capabilities to follow individual particles as a function of time while providing 3D particle positions and velocities.[19–23] The 3D-PTV system is based on the acquisition and processing of a sequence of images, of a particle seeded flow, from several cameras with different orientations. Compared with PEPT and CAEPT techniques, this optical flow diagnostic technique is less complex, less expensive as well as more accurate and robust, and able to track a larger number of suspended particles (in a clear fluid) at any given time.

The present description of the research begins with a discussion of the mathematical theory of the 3D-PTV technique and the experimental methods. Validation and accuracy of the system are then described. The results section follows, including a comparison of the 3D-PTV technique with a conventional single PIV system. Finally, quantitative flow measurement results using a 3D-PTV system in a custom-made stirred tank will be shown.

3D Particle Image Reconstruction

3D-PTV is a powerful flow measurement technique that is able to locate the 3D spatial position of individual particles, by interpolating images between two or more cameras using epipolar geometry, and tracking the change in position as a function of time. The 3D particle position reconstruction process can be described as follows. First, it requires simultaneously imaging the suspended particles in the flow with two or more cameras from different perspectives. Next, the captured gray-scale images are processed to indentify the centroid of individual particles in the image plane. Finally, through a reconstruction geometry process (epipolar geometry) that will be discussed next, the particle position is converted between the two-dimensional image plane (plane where the CCD sensor of a camera is located) and the three-dimensional world coordinate system (coordinate system based on the volume being observed).

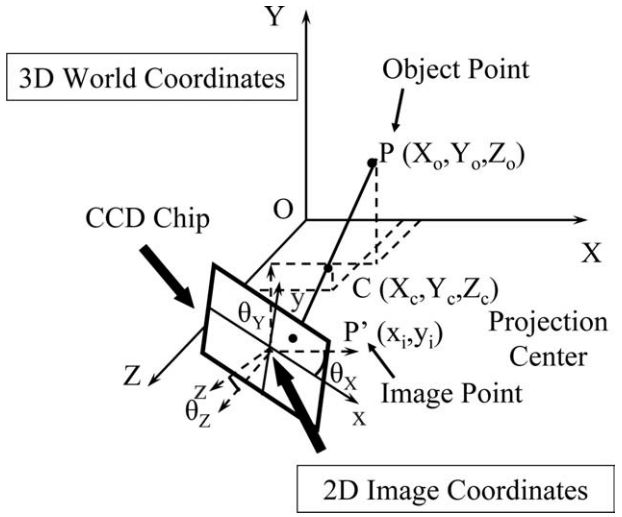

Figure 1. Sketch of the projection of an objection point from 3D world coordinates to 2D Image coordinate in the camera.

3D Reconstruction from a single camera image

The simplest case of 3D geometric reconstruction (from a 2D image plane to a 3D world coordinate) is shown in Figure 1 by the correlation between an object and an image of the object taken with a single pinhole camera. The figure shows the projection of the object from the 3D world coordinate system (X, Y, Z) to the 2D image coordinate system (x, y). The light reflected from the object point P, passes through the small aperture pinhole of the camera and forms an image point P', on the camera image plane. This is the perspective projection, which is defined as the projection of a three-dimensional object onto a two-dimensional surface by straight lines that pass through a single point or pinhole, labeled C in Figure 1.[24] The perspective projection from the physical object point P (X_o, Y_o, Z_o) to the image point P' (x_i, y_i) is given by

$$\begin{pmatrix} w_i x_i \\ w_i y_i \\ w_i \end{pmatrix} = \begin{bmatrix} a_{11} & a_{12} & a_{13} & a_{14} \\ a_{21} & a_{22} & a_{23} & a_{24} \\ a_{31} & a_{32} & a_{33} & a_{34} \end{bmatrix} \begin{pmatrix} X_o \\ Y_o \\ Z_o \\ 1 \end{pmatrix} \tag{1}$$

where the 3D space is represented by a 4×1 vector in homogenous coordinates by introducing a nonzero and arbitrary constant w. The equation can be rewritten as:

$$x_i = \frac{w_i x_i}{w_i} = \frac{a_{11}X_o + a_{12}Y_o + a_{13}Z_o + a_{14}}{a_{31}X_o + a_{32}Y_o + a_{33}Z_o + a_{34}} \tag{2}$$

$$y_i = \frac{w_i y_i}{w_i} = \frac{a_{21}X_o + a_{22}Y_o + a_{23}Z_o + a_{24}}{a_{31}X_o + a_{32}Y_o + a_{33}Z_o + a_{34}} \quad (3)$$

The coefficients a_{ij} in the 3×4 conversion matrix are nonlinear functions of the camera focal length f, camera projection center position X_c, Y_c, Z_c, camera body rotation angles θ_X, θ_Y, θ_Z, and other lens distortion and decentering distortion parameters.[25] These unknown coefficients can be obtained from a calibration process, which uses a calibration target with reference marks, such as white dots, with an a priori known 3D position. When applying a 3D geometric reconstruction algorithm to 2D images, the particle position in the image coordinates (x_i, y_i) is a known variable, while the real position of the particle (X_o, Y_o, Z_o) is unknown. The solution for a single camera configuration is not unique, as there are three unknowns and only two equations, Eqs. 2–3. This requires a second camera, with a different perspective, to solve the system of equations and allow 2D to 3D reconstruction.

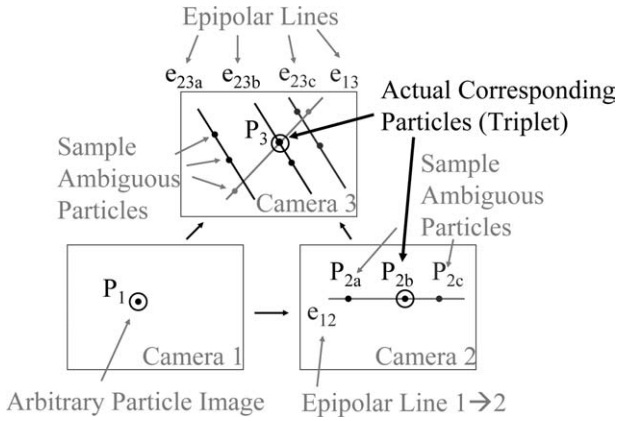

Figure 2. Sketch showing that when using epipolar geometry the position of a point in one camera is constraint in the other two along epipolar lines (three camera correspondence).

3D Reconstruction from multi-camera images and particle correspondence

The process of reconstructing an object in 3D space from a pair of stereo images (two cameras) using epipolar geometry is well documented in the literature especially for machine vision.[26-28] It states that if two camera (CCD planes) positions and orientation are known in World Coordinates and if they are also both imaging the same volume, then epipolar geometry shows that the projection of a point in one camera is constraint in the second camera and can only be found projected along a line (epipolar line). However, the recognition of a stereo pair of image points becomes a problem, as there can be multiple ambiguous particles (solutions) found along same epipolar lines. Thus, the two camera image reconstruction suffers from low accuracy, reliability and occlusion effects. This is known as an issue of correspondence (i.e., accurately matching a point in both cameras) which is a very significant problem found in 3D-PTV, due also to the large depth of volume being observed (10–100 mm), with relatively high concentration of tracer particles (100–1000 particles per volume), and where the particles only occupy a few pixels in the cameras.

To decrease the number of ambiguous particles and the accuracy of the system, a third camera is introduced. As shown in Figure 2, the correspondence of an arbitrary image point P_1 in the first camera, can be found along the epipolar line e_{12}, in the second camera identified by, for example, P_{2a}, P_{2b}, and P_{3c}. The three candidates produce three epipolar lines e_{23a}, e_{23b}, and e_{23c} in the third camera, while P_1 produces an epipolar line e_{13} in the third camera. The correspondence can be found by looking for the intersection between e_{23a}, e_{23b}, e_{23c}, and e_{13}, which defines a triplet. The third camera can decrease the number of possible candidates by a factor of 10, but there are still ambiguities that make the correspondence nonunique. The introduction of a fourth camera can decrease the number of ambiguities by a factor of 100, when compared with the stereo setup, and the uniqueness of the quadruplets (intersection of epipolar lines for a point from all cameras) is achieved. A full quantitative analysis and formulation to show the number of ambiguous particles, that depends on the epipolar geometry and the number of cameras can be found elsewhere.[29] For instance, in one case Maas (1992)[30] shows that a two camera arrangement produces over 401 ambiguities (solutions) for each searchable particle. For instance, analysis have shown that the number of ambiguities for two cameras is of the order of 400 and that this can be reduced to 35–40 for a three camera arrangement and close to zero for a four camera arrangement.[29] This shows that although more cameras could be used beyond four cameras, they are not necessary as they scarcely contribute to improve the accuracy of the system.

Image analysis

The 3D particle position reconstruction process only considers the particles detected in three and four cameras (triplets and quadruplets) as valid particles, since the ambiguity is sufficiently small. Particles detected in only two cameras are discarded. The next processing step considers correlating detected particles in the time domain. Given an instantaneous 3D particle position, its position at the next time step is predicted if the position at the previous time step is known. In reality, the previous time step position is not known so an iterative process is needed that requires a backward-projection correction. During this process some limitations should be considered. First, the particle position in the backward and forward time step should not have changed (in the three or four cameras) more than a few pixels which truly limit the speed of the flows that can be studied (limited by the maximum camera frame rate). Second, the back projection of the 3D particle search position might result in multiple candidates requiring a prediction of the 3D search position for each one of them in the forward step (this limits the particle concentrations and maximum displacement that the system can handle). Once a particle is matched on each camera at both the previous and the next time step, the particle is considered to be valid in the time domain and its 3D position is recorded. The 3D position is again analyzed through the same procedure to acquire the information for the next time step. The present work uses this method via an algorithm developed and obtained from ETH Zurich (Swiss

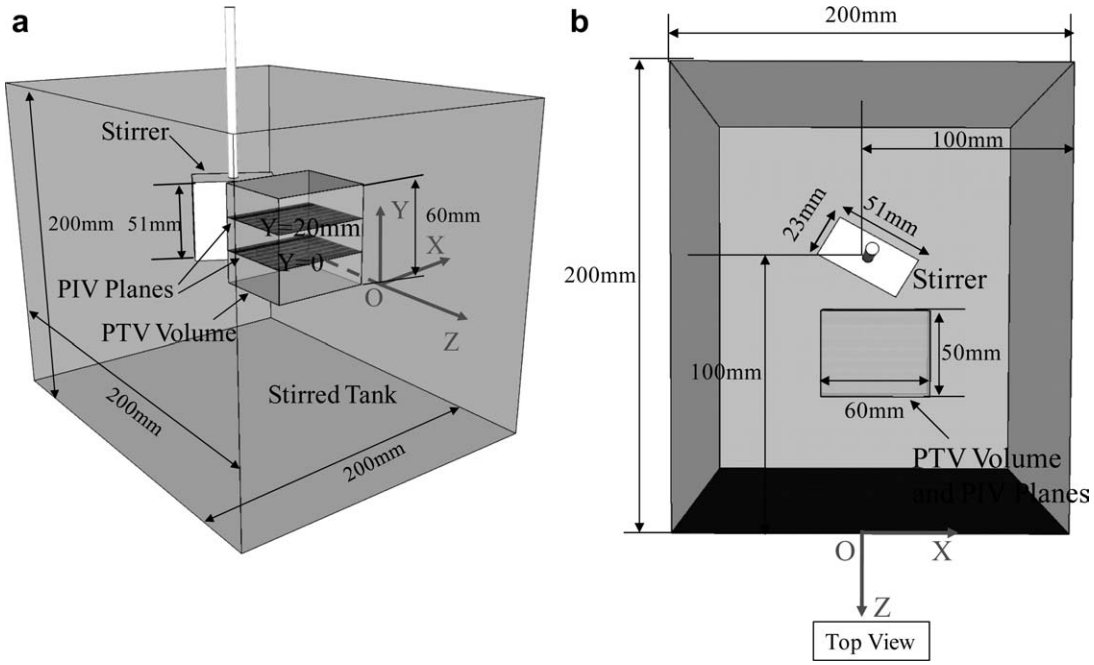

Figure 3. (a) Front perspective view of stirred tank and (b) its top perspective view (the somewhat angled away view makes the stirrer seemed off-centered but it is not) illustrating the location of the observation planes and volume (for 2D-PIV and 3D-PTV measurements).

The stirrer rotates clockwise next to the observation volume.

Federal Institute of Technology).[21,25] This method allows detecting the 3D particle positions in adjacent time steps, which when linked together produce trajectories of the particle and can be further analyzed to obtain the 3D velocity field, and even particle accelerations.

Experimental Methods

Experimental setup

Description of the Stirred Tank. First, the 3D-PTV system will be validated in a 1D setup and then its 3D time resolved diagnostic capabilities applied to a custom-made stirred tank. A sketch of the tank setup including the location of the PTV observation volume with respect to the stirrer is shown in Figure 3. The stirrer dimensions were 51 mm × 51 mm × 23 mm, and it was made of clear acrylic. This material was chosen for having an index of refraction ($n = 1.49$) very similar to that of glycerin ($n = 1.473$) used as the working fluid. By having a very similar index of refraction the stirrer optically disappears in the fluid. This greatly reduced the reflections produced by any laser light hitting the stirrer and allows observation volumes that can overlap with the stirrer. The stirrer was driven by a gear motor at a constant rotation speed of 6 rpm (N_{rps}).

Test Conditions. Test conditions for the 3D-PTV measurements in a stirred tank are summarized in Table 1. The experiment involved two tank configurations with the main one corresponding to a square tank (200 mm × 200 mm) with the stirrer positioned in the center, and another corresponding to a rectangular tank (300 mm × 150 mm) with the stirrer positioned off-center in the Z direction ($X_{stir} = 0$ mm, $Z_{stir} = -100$ mm). Other overall test conditions were as follows: Reynolds number of 23.6 ($Re = \rho N_{rps} D^2/\mu$), aluminum oxide particles of 100 microns and particle seeding concentration of ~6 particles/cc. The concentration of particles provided a particle distribution of about 1000 particles in each image with a total detected number of particles of ~395 (triplets and quadruplets).

Experimental technique

3D-PTV System Setup. A synchronized image acquisition system was developed for time-resolved 3D capture of the suspended particles in a mixing stirring tank. The system setup consists of four charge-coupled device (CCD) cameras connected to two synchronizers and two PC computers as shown in Figure 4. The illumination source used was an Nd:YAG laser, with the laser beam expanded via a liquid light guide and cylindrical lenses producing a homogeneous volume illumination of the fluid. The four cameras were

Table 1. Summary of Test Conditions for the Stirred Tank Measurements*

Parameters	Mixer
Working fluid	Glycerin
Seeding particle	Al_2O_3
Seeding particle diameter (μm)	100
Density of fluid (ρ) (g/cm^3)	1.26
Density of particles (ρ) (g/cm^3)	4.0
Kinematic viscosity of fluid (μ), (Pa s)	1.5
Rotation diameter stirrer (D) (mm)	51
Rotation speed of stirrer (N_{rps}) (rpm)	6
Particles (per cm^3)	5.5 ± 0.5
Detected particles (triplets & quadruplets)	395 ± 40

*Ambient and fluid temperature of 297 ± 0.5K.

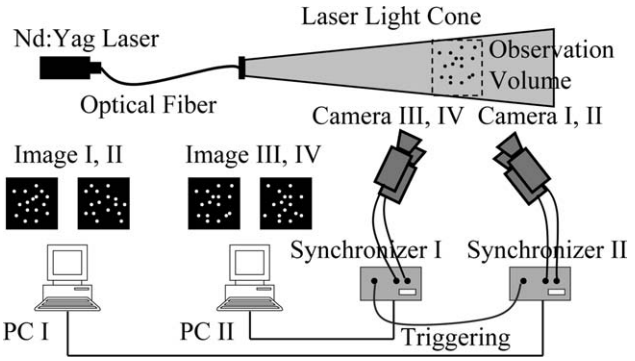

Figure 4. Experimental setup for 3D-PTV data acquisition system.

oriented and focused onto the same region of the illuminated volume. This is known as the observation volume. The four cameras are synchronized using two digital delay generators so they can capture images simultaneously. The acquired images are transferred to two computers via individual frame grabbers for each camera. Two computers were needed to allow for enough bandwidth for real time and continuous transfer of the data. The output of the acquisition system consists of a time resolved series of particle images from each of the four cameras which observe the particles in the measurement volume from four different perspectives.

The cameras used were Kodak MegaPlus ES 1.0, with capture rate of 15 frame/s, image resolution of 1008 × 1024 pixels, active CCD sensor area of 9.1 mm × 9.2 mm, and fitted with Nikon 50 mm f/1.8 AF lenses. The four cameras were mounted on three degrees of freedom mounts. The illumination source used was a New Wave Solo PIV Nd:YAG Laser with a repetition rate of 15 Hz, energy of 120 mJ at 532 nm wavelength, and a nominal beam diameter of 5 mm. In order to obtain a uniform laser light intensity distribution (the beam has a quasi-Gaussian intensity distribution) the beam was sent through a Newport Liquid Light Guide. This created a homogeneous and uniform laser beam exiting the Light Guide which was expanded into the desired size volumetric light cone using two concave cylindrical lenses with 15 mm focal length and 25 mm focal length placed with optical axis orthogonal to each other. The laser power was adjusted so that the homogeneous light cone illuminated the particles in the stirred tank with enough intensity for them to scatter enough light to be detected by the CCD cameras. Also, the laser pulse duration was very short, 3–5 ns, which allowed the camera images to "freeze" the particle motion at one time step without producing a streaking effect typical of longer exposure illumination systems. The cameras were operated at their maximum frame rate (15 fps) for all the present work. This hardware constraint (easily overcome with current generation of high speed cameras) limited the application of our system to only low Reynolds number (<50) flows (i.e., low speed stirrer in a glycerin filled tank) to prevent particle displacements of more than a few pixels between different consecutive time steps so they can be correlated accurately by the 3D-PTV software.

2D-PIV System Setup. The 3D-PTV measurements are compared and validated with measurements from a conventional 2D-PIV system. The 2D-PIV arrangement consists of an Nd:YAG laser (New Wave Solo PIV), a CCD camera (Kodak MegaPlus ES 1.0), a synchronizer (TSI 610034 LASERPULSE Synchronizer), and a PC with TSI Insight 3G software to process the PIV images. A cylindrical lens and a spherical lens are used to create a 1 mm thin laser sheet to illuminate the imaging plane (60 mm × 60 mm) as shown in Figure 5a. This is in contrast to the observation volume (60 mm × 60 mm × 50 mm) that is used for the 3D-PTV measurements as shown in Figure 5b. A sketch of the location of the 3D-PTV observation volume and the 2D-PIV measurement plane in reference to the stirrer is shown in Figure 3.

3D-PTV System calibration

To reconstruct the 3D position of particles in the observation volume from the four camera images, a conversion algorithm between the image coordinate system and the

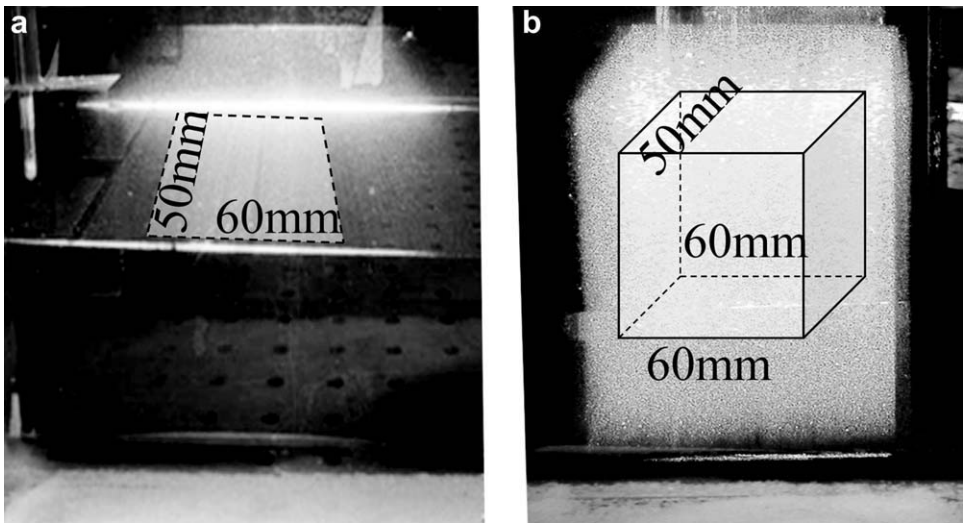

Figure 5. Comparison of laser illumination showing, (a) laser sheet for 2D-PIV system and (b) laser volume for 3D-PTV system.

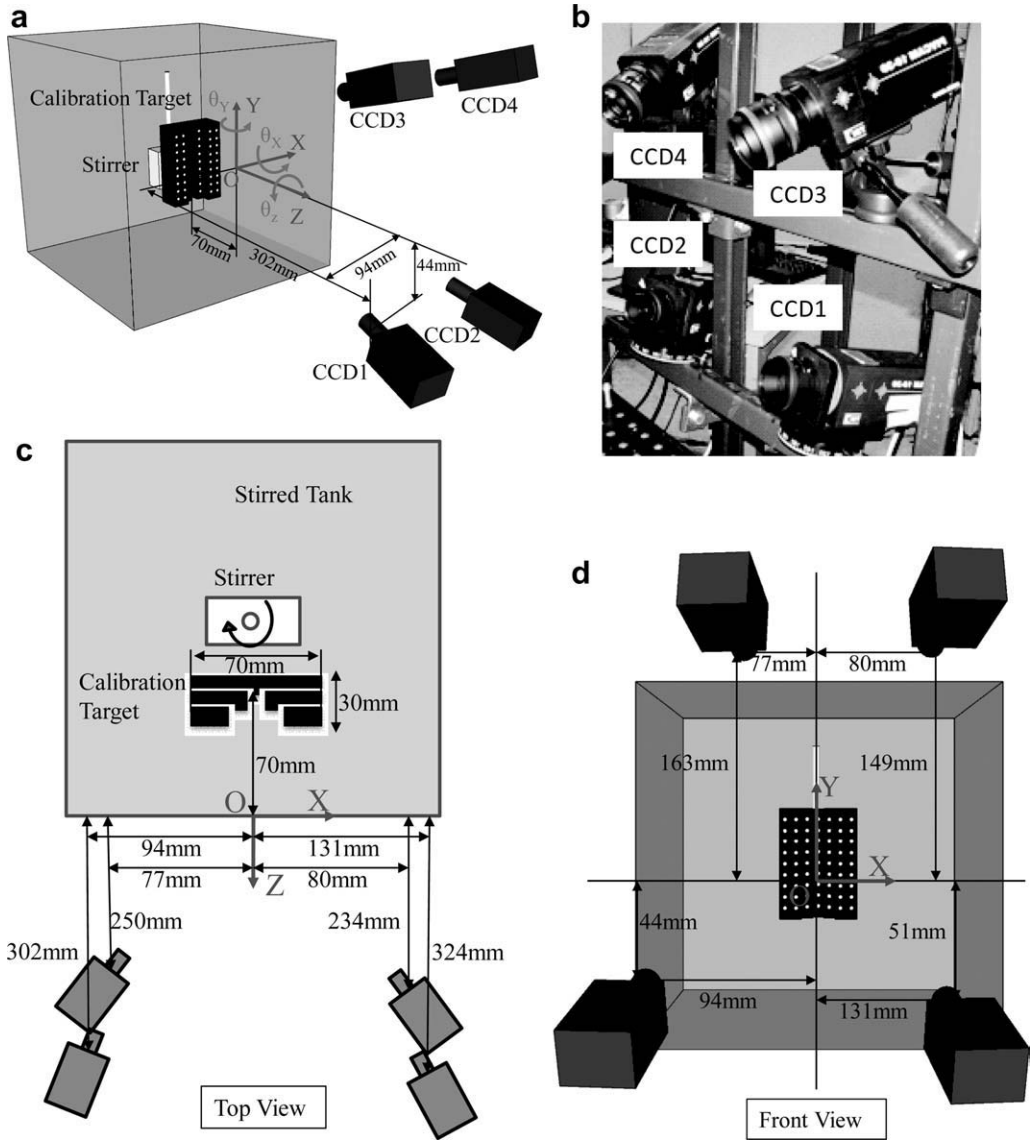

Figure 6. Sketch showing the location of the calibration target and the four cameras in reference to the world coordinates (*X*, *Y*, *Z*) in (a) perspective view, (b) inset showing photograph of actual camera setup, (c) top view, and (d) side view.

world coordinate system is needed. The algorithm is based on epipolar geometry reconstruction and requires a set of coefficients that are nonlinearly dependent on the physical setup parameters of the cameras with respect to the measurement volume. These parameters include the location of the camera projection center position X_c, Y_c, Z_c, and camera body rotation angles θ_X, θ_Y, θ_Z. These parameters are shown in Figure 6 in world coordinates system with the origin of the system set on the outer wall of the measurement tank. It should be noted that the parameters also depend on the camera focal length f, and the properties and possible distortions of the lens.

The most direct method to obtain the coefficients involves a calibration procedure where a 3D calibration target is introduced in the measurement volume as illustrated in Figure 6. The calibration target contains a set of reference marks (dots) with known 3D positions in world coordinates. After building a variety of 3D targets, it was found that for best results the calibration target should have dimensions comparable with the observed volume, with sufficient marks (50–100 marks), and the marks should spread over the entire observed volume as opposed to being contained in a single 2D plane. For system calibration, the target is placed at the observation volume and the position of each reference mark in the world coordinate is measured. Accurate knowledge of the position of these marks is needed to minimize any errors in calculating the camera parameters. The calibration is then performed by taking a set of images of the 3D target from the four different perspectives of the four cameras. From these images, a transformation matrix is generated that relates the known position of the target marks in world coordinates with their position in the image coordinate system. For the present experiment, the physical dimensions of the optimized calibration target were 100 mm × 70 mm × 30 mm, with 70

Table 2. 3D PTV Camera Geometrical Configuration for Three Cases Studied

	Position* (X,Y,Z), mm			Angle (θ_x, θ_y, θ_z), °		
	Case I	Case II	Case III	Case I	Case II	Case III
CCD1	−82,1,347	−96,−38,772	−94,−44,302	3,−11,−1	3,−6,0	12,−14,0
CCD2	27,0,337	64,−16,765	131,−51,324	5,5,−1	3,6,0	13,21,−1
CCD3	−76,440,228	−272,282,729	−77,163,250	−24,−12,−7	−19,−17,−7	−25,−12,5
CCD4	38,144,235	188,256,702	80,149,234	−24,9,2	−19,15,3	−24,17,7

*Global coordinates.

reference dots on it. The spacing between the dots was 10 mm. The calibration target was painted black and had white reference dots, so that the high intensity contrast makes the location of the reference dots more accurate on the calibration images.

3D-PTV Accuracy

After considering the effect of the calibration process into the accuracy of the 3D-PTV measurements, it was also found that the accuracy was very sensitive to the type of particles, the observation volume illumination, and the camera orientation. The influence of these different components into the accuracy of the system was studied using a simple 1D flow generated by the motion of piston configuration.

Influence of Particles and Illumination. Before considering the results of the particle motion under the piston-generated flow, some general guidelines were set from preliminary tests. In terms of the properties of the the particles used, the following were preferred when possible: (a) particles with enhanced light scattering ability are favored so they can be easily detected by the camera image sensors (this also depends on camera sensor sensitivity); (b) if passive tracer particles are needed to study the flow characteristics, their size should be small enough to represent the flow motion and large enough to scatter adequate amount of light;[31] (c) for best results, particle size needs to be matched with laser light intensity and/or size of the observation volume for a given camera/lens system so sufficient laser light reaches the camera from each particle; (d) spherical particles are preferred for uniform light scattering abilities which facilitates particle centroid identification within the 3D-PTV software; (e) individual particles should occupy at least 5–10 pixels in the CCD sensor (even larger is desired) which helps finding particle correspondence in the other three cameras using epipolar geometry. In terms of the observation volume, it was found that a homogenous volume illumination produced the best results. In some cases, a white light source could be used for flood illumination but an Nd-YAG laser light was preferred for highest light intensity per pulse delivered. A series of optics and a liquid light guide were used, as described in Section 3.2, to create the desired volume. This illuminated volume should match the observed volume. Limitations on the size of the observed volume depend on maximum light intensity available and camera properties such as resolution, size of CCD chip, and lens aperture range.

Influence of Camera Configuration. Camera configuration refers to the arrangement of the four cameras in the 3D-PTV system in terms of their spatial location. The arrangement of the cameras has a significant influence on the establishment of particle correspondence between images and the accuracy of the system.[29,32] This is of particular interest for the present work where the size of the observed control volume is the largest, to our knowledge, reported to date in the literature, which required careful optimization of the camera configuration.

Multiple camera configurations were considered, with the geometry arrangement for the top three cases studied shown in Table 2, and their accuracy compared in Table 3. The geometrical configuration for the four cameras, for each case studied, is given in world coordinates and in terms of the camera orientation and rotation angles as defined in Figure 6. Briefly, the cameras were mounted onto two parallel horizontal bars, with two cameras on the top bar and two on the bottom. Each camera uses a three degrees-of-freedom tripod mechanism mounted to the bar which allowed the camera to be oriented and rotated independently. For the first camera configuration (Case I), the bottom two cameras were placed with small θ_x angles, and all four cameras were closer to each other than the other two cases, and with short distances to the observed volume. This configuration benefits from having the largest overlapping field of view area among the four cameras (i.e., most of the CCD area in all cameras is imaging the observed volume) and produces the largest percentage of quadruplets when compared with the other configurations. The second camera configuration (Case II) introduces the largest separation between the four cameras which allows observing the measurement volume from very different perspectives. Since the top two cameras (CCD3 and CCD4) are the farthest apart from each other, they observe a larger area than the bottom two cameras. To match their field of view magnification, they were moved forward. The third camera configuration (Case III) has the four cameras in a square arrangement with similar θ_x and θ_y angles. This configuration was a compromise between trying to provide a

Table 3. Accuracy of 3D PTV System for Three Geometrical Configurations of the Cameras

Camera Configuration	ΔX_{error} (%)	ΔY_{error} (%)	ΔZ_{error} (%)	Quadruplets/Total Particles (%)	Linked/Total Particles (%)
Case I	0.27	0.34	1.31	49.8	26.2
Case II	0.10	0.13	0.53	6.56	54.8
Case III	0.10	0.11	0.39	29.2	66.6

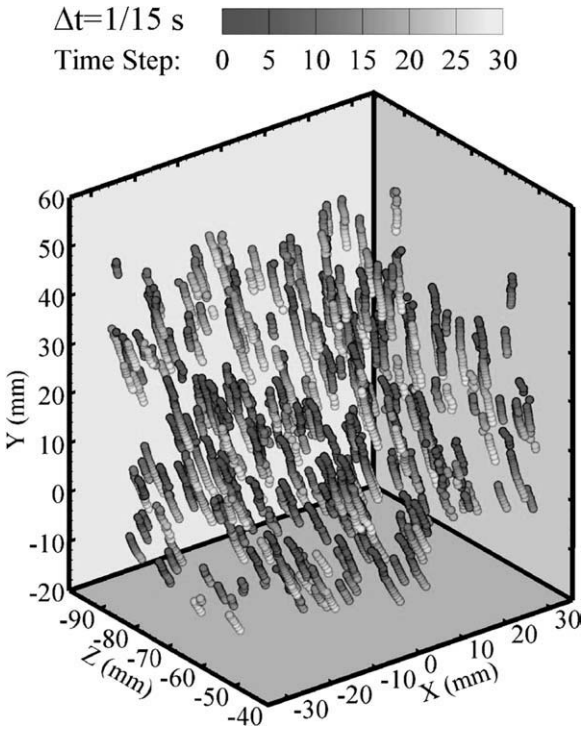

Figure 7. Selected 3D particle trajectories obtained with the 3D PTV system.

Color coding represents the different time steps. Vertical motion was generated by a piston with the particles closely following a vertical trajectory.

larger overlapping field of view between the four cameras and also trying to provide different camera perspectives for improving the camera calibration transformation discussed in Section 3.3.

The following three aspects were considered in the 3D PTV accuracy study (Table 3) of the different camera configurations: (a) error in estimating a particle location, (b) total number of quadruplets found, and (c) ability to track a particle during multiple time steps. First, the error in estimating a particle location (triplet or quadruplet) in world coordinates is considered. Table 3 shows that Case I is the least accurate in determining particle positions. This is due to the short distance between the cameras, which results in images without enough stereoscopic disparity in the z-direction. This effect increases the error of the z-component during the 3D particle position reconstruction. Second, particle correspondence is compared for the three cases. It is shown that Case I has the largest number of matching particles detected simultaneously by four cameras (quadruplets), due to the large overlapping field of view of this configuration. The poor correspondence in Case II is caused by the large varying particle shape/size observed by cameras far apart from each other which makes it more difficult for the correspondence process between the four cameras. Table 3 also indicates that Case III has the best ability to track each single particle through different time steps. The comparison between the three cases shows that Case III has the best performance overall, with the smallest particle location error, and the most number of particle trajectories which ultimately provides the better Lagrangian particle description. Therefore, the final camera arrangement used for all the 3D-PTV measurements in the following was given by Case III.

Results

Test results for 1D flow

The 3D-PTV system was first tested on a quasi 1-D flow generated by a large moving piston. This produced a constant velocity of 15 mm/s in a rectangular tank filled with glycerin. The observation volume (60 mm × 60 mm × 50 mm) was located in the center of the tank. Since the constant speed of the piston is known, it was possible to validate the velocity results obtained with the 3D-PTV system. These were better than 1 percent for V_x, V_y, and V_z. The small differences were attributed to the use of large particles (100 microns) which do not accurately follow the flow and slow sink at rest. Typical 3D particle trajectories are shown in Figure 7. The different color shades indicate particle positions at different time steps. The figure shows the visualization of individual particle trajectories in the observed volume for up to 50 time steps. On average, 400 particles could be tracked at any given time.

Comparison with previous work

Although the concept of 3D-PTV is not new,[33] only a reduced group of researchers have published work using this 3D Lagrangian Particle Tracking technique. This is due in part to the cost and complexity of the hardware setup required, but also due to the large development time needed to produce accurate results. Thus, it is important to compare the accuracy of the obtained 3D-PTV results to other previous published work to ensure that similar accuracies can be obtained indicating that the system was fully developed. One of the key features of the present 3D-PTV measurements is the size of the observation volume, which is larger than any other previous published work. This was done in order to observe particle trajectories in a mixing stirred tank. The statistic results of this setup are compared in Table 4 with available literature data[25] (3D PTV data set compared was obtained from that work through private communication with the ETH personnel in acknowledgement) where a magnetically driven flow with charged copper sulphate in a large observation volume of 20 mm × 20 mm × 20 mm was studied. Both flows had very similar conditions including particle density, motion of particles between frames (i.e., 6 pixels) and particle links, but their data was taken at a faster rate (60 fps). Also, the present work observed a measuring volume nearly nine times larger than previously reported.[25] Results show that the error associated with finding the

Table 4. Statistic Test Results Comparison Between the Present 3D PTV Work and Wilneff[25]

	Present 3D-PTV System	Wilneff[25]
Links/particles	68%	65%
ΔX_{error}	0.10%	0.05%
ΔY_{error}	0.11%	0.05%
ΔZ_{error}	0.39%	0.16%
Dimensions of observation volume	60 mm × 60 mm × 50 mm	20 mm × 20 mm × 20 mm

particle location was only two times greater and well within the expected range for 3D-PTV while the ability to track single particles was very similar in both cases. Once the hardware setup is optimized, we believe that these statistical similarities observed are connected to the capabilities of the code used in the analysis (the same code was used for both cases and its capabilities are much improved over earlier work[29]). This comparison test was an important part of the accuracy study and indicates the capability of the developed 3D-PTV system.

Validation of 3D-PTV measurements using 2D-PIV

The use of PIV as a tool to perform CFD validations and study flow fields of stirred tanks is well established in the chemical process industry.[34-36] As such, a 2D-PIV system was used to measure the velocity field and the results compared with those obtained with the 3D-PTV system developed. For both systems, 10 sets of 75 images pairs were taken, which corresponds to tracking the flow for half a revolution per set for a total of five revolutions for the 10 sets. Data acquisition for all PTV and PIV data sets were always started with the same stirrer location (parallel to the volume). Other test conditions are shown in Table 1 and were the same for both the PIV and PTV methods. The only exception corresponds to the PIV particle seeding concentration used in the tank which was about 50 times higher than for 3D-PTV. This is due to the statistical nature of PIV, where each velocity vector is the result of the individual cross correlation of two interrogation windows (typical sizes used were between 32 pixels $\times$ 32 pixels and 64 pixels $\times$ 64 pixels) from two consecutive images. An interrogation window should have a minimum of six good particles (particles that stay within the interrogation windows in both frames) for proper correlation to produce a vector. Depending on the size of the interrogation window, a 2D-PIV image (1024 pixels $\times$ 1024 pixels) should have a minimum of 1500 particles to 6000 particles. On the other hand, the velocity field of the 3D-PTV system is obtained from individual particle positions reconstructed using epipolar geometry which puts a constraint in the maximum number of particles that can be tracked in each volume. Experiments show this to be around 400 particles for the present conditions. This explains the large seeding differences between both techniques.

Velocity measurements with the 2D-PIV system were obtained in two planes perpendicular to the stirrer, as shown in Figure 3. Results for both planes were the same. These results are indicative of the flow not changing in the vertical direction at least within the height of the stirrer. This is expected for such a low Reynolds number, revealing the quasi 2D characteristics of this stirred flow. A typical instantaneous 2D velocity contour plot obtained with the PIV setup is shown in Figure 8a with the axes given in global coordinates as defined in Figure 3. The plot shows that the flow was rotating clockwise around the y-axis in a near circular trajectory and with a range of velocities observed from 2 to 8 mm/s. It should be noted that the high density difference between particles and fluid creates a slightly off vertical velocity corresponding to a terminal velocity of the particles (0.067 mm/s) which is negligible when compared with their imparted speed by the stirrer. The center of rotation of the stirrer was at $X = 0$, $Z = -95$ mm, and along the y-axis. On

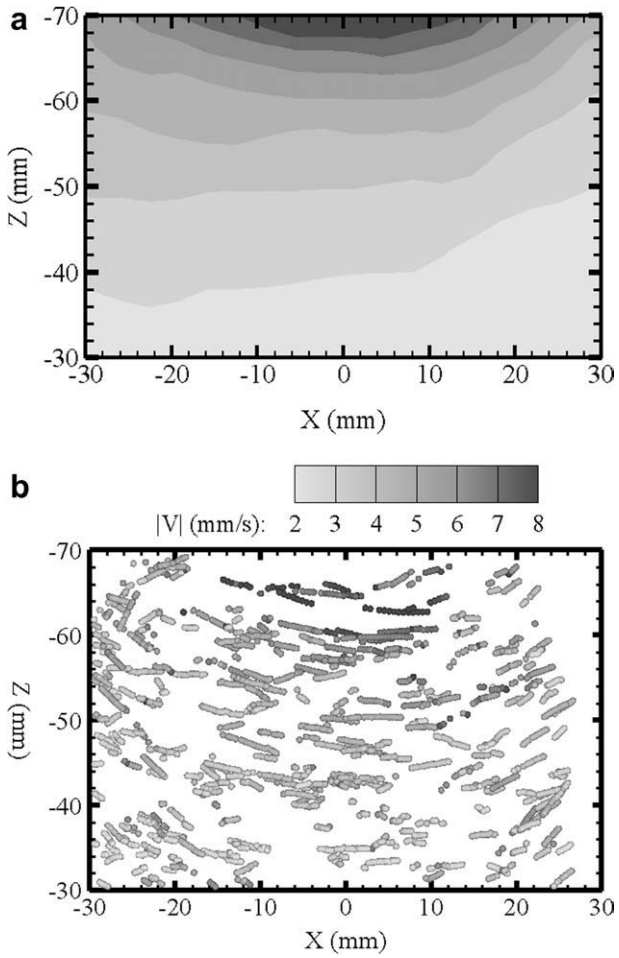

Figure 8. The comparison of velocity magnitudes are shown (a) in contour plot form for the 2D-PIV results and (b) as individual particle velocities with their trajectories for the 3D-PTV results.

the other hand, it was not possible to generate velocity contour plots with the 3D-PTV system, given the relatively small number of particles that it can track in any given volume. But the 3D-PTV system generates 3D particle velocities with their trajectories that can be quantitatively compared with the PIV contour plots. Figure 8b shows individual particle velocity magnitudes and trajectories for up to 50 time steps. Each solid circle in the figure represents a particle position and its color represents its velocity magnitude. A connected chain of circles represents the particle trajectory with the colors giving the velocity variation of single particles as a function of time. The top view (XZ plane) of the 3D-PTV observation volume is given in Figure 8b, with particles rotating clockwise in the direction of the stirrer and describing a circular trajectory similar to Figure 8a. Thus, good agreement was observed between the PIV velocity contour plot and the 3D PTV particle velocities. Finally, Figures 8a, b also shows that the flow is laminar with the highest velocity near the center, where the axis of rotation of the stirrer is located, and the velocity decreases radially outwards.

A detail comparison of the velocity magnitudes obtained from the two systems is plotted in Figure 9. The solid lines

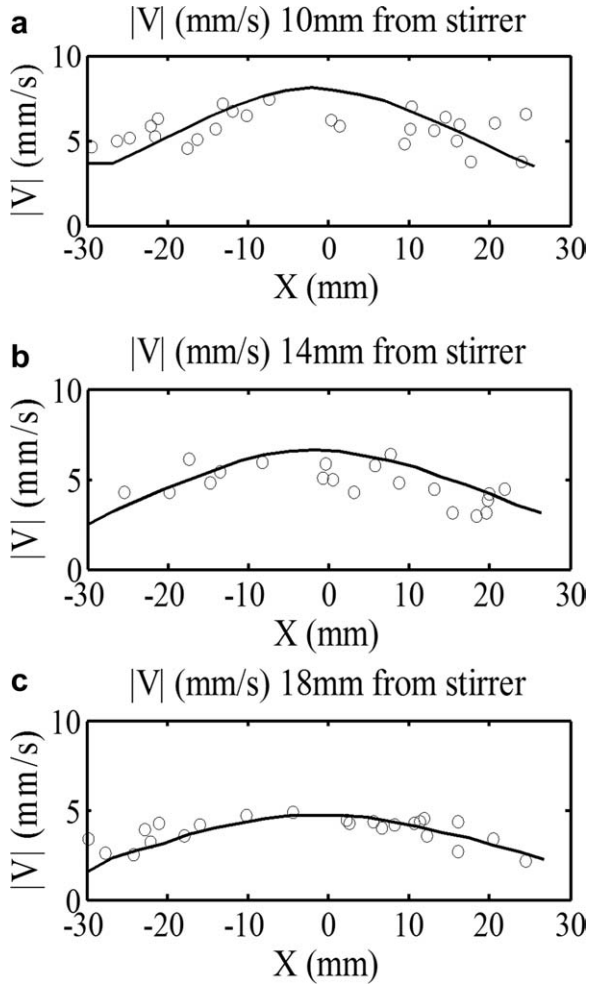

Figure 9. Comparison of measured velocity magnitudes along the *X*-axis and *Y* = 0, at several distances from the stirrer.

The solid lines represent the PIV-obtained velocity magnitudes and the open circles represent the 3D-PTV obtained velocity magnitudes.

represent the PIV-obtained velocity magnitudes (average form 150 images) and the circles represent the 3D-PTV obtained velocity magnitudes. Results are given at 35, 39, and 42 mm from the center of rotation of the stirrer which corresponds to the planes $Z = -50$, -46, and -42 mm, respectively. At these Z-locations, Figure 9 shows that only a few particles were found using 3D-PTV, which is the result of the number of particles the PTV system can track in a volume at any given time ($\sim$400). This was expected, as the main characteristic of the PTV system is not to provide velocity profiles but rather accurate description of the trajectories of individual particles. Nevertheless, these results indicate that the 3D-PTV and PIV techniques observed the same flow motion, with similar magnitudes and flow behavior. An observation should be made that in order to produce average 3D-PTV results similar to the instantaneous PIV velocity results shown in Figure 8a, over 500 data sets should be taken instead of the 10 used for this comparison. This was beyond the scope of this work given the processing time needed. This also suggests that the strength of PTV is not in producing average velocity fields but in providing Lagrangian particle tracking as will be discussed next.

3D Particle trajectories, velocity, and acceleration

After comparing the velocity results with 2D-PIV, the 3D-PTV system was applied to study the 3D particle trajectories generated by two stirrer configurations. For the base configuration, the stirrer was positioned in the center of a square tank (200 mm $\times$ 200 mm) and this symmetric configuration generated quasi-circular particle trajectories. This is illustrated in Figure 10a and it represents the 3D view of the results shown in Figure 8 (X–Z view) where particles were tracked for up to one-half revolution. For the second configuration, the stirrer was positioned off-center in the Z direction ($X_{stir} = 0$ mm, $Z_{stir} = -100$ mm) in a rectangular tank (300 mm $\times$ 150 mm) and generated a nonsymmetric flow pattern. This produced a variety of 3D trajectories as illustrated in Figure 10b. Figures 10a, b show, in global coordinates, the 3D position of the particles in the flow near the stirrer. Each solid circle in the figure represents a particle position and its filled-color represents a time step such that all the particles observed at the same time step have the same color. The figure shows up to 50 time steps and each chain of connected circles represent a Lagrangian particle trajectory. By observing the length of the trajectories, one can infer the speed of the particles (sorter chains indicating the lower speed of the particle than for larger chains). Figure 10b shows that the particles near the stirrer (i.e., $-90 < Z < 70$, $0 < Y < 60$) move clockwise (red to yellow) in the direction of the stirrer while those further away (i.e., $-90 < Z < -70$, $0 < Y < 60$) follow a downward secondary flow produced by the nonsymmetric arrangement of the stirrer.

By knowing the particle position between two consecutive time steps, the particle velocity can be obtained. This is illustrated for the symmetric and nonsymmetric configuration in Figure 11, where particles' velocity magnitudes are shown for up to 50 time steps. Note that the colors for each particle (connected circles) correspond to its velocity magnitude changing in time. Both configurations show, as expected, the circular flow motion generated by the stirrer with velocities decaying as one moves radially outwards from the stirrer. This capability of the 3D-PTV system to show the instantaneous three-dimensional particle velocities is important to studying mixing in stirred tanks. First, it complements techniques like PIV, which are only capable of performing planar measurements, by providing instantaneous velocity in the full observation volume. Second, by tracking individual particles in a volume, it provides particle position and velocity as a function of time. This Lagrangian way of describing the flow can provide a more natural way of comparing and validating results with most CFD Lagrangian models available. This method can also lead to understanding which region of the flows are not mixed well, and what type of forces are the particles experiencing in different regions of the tank.

By knowing the change of velocity magnitude of individual particles for two consecutive time steps, the particle acceleration can also be obtained. This is illustrated for the quasi-1D piston generated flow in Figure 12. The figure shows selected particles accelerating or decelerating

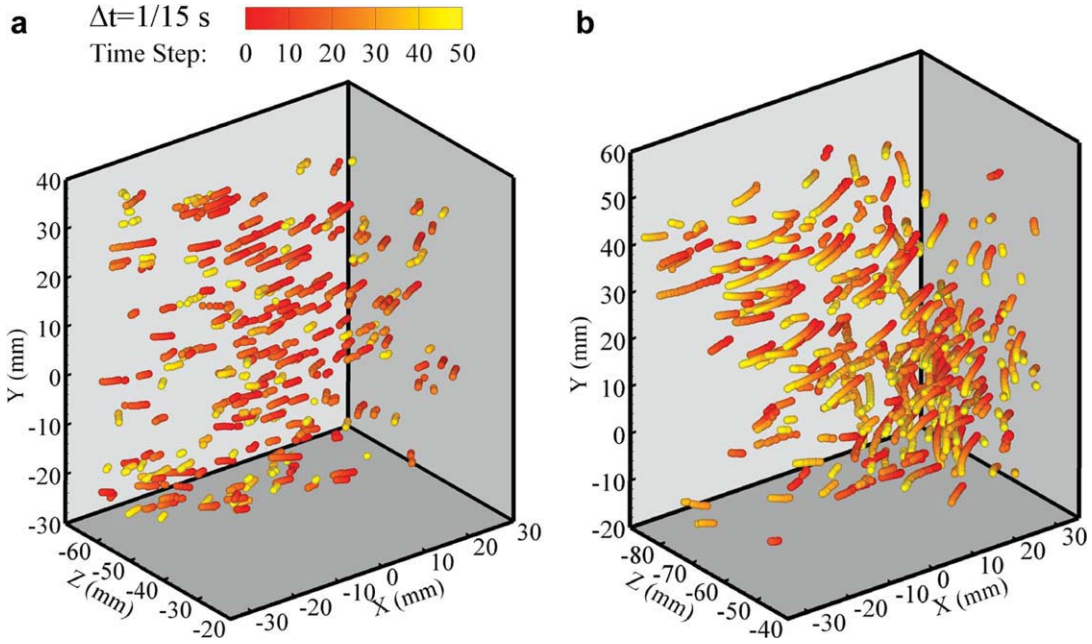

Figure 10. 3D plot of the particle trajectories in the observation volume for the flows generated by (a) the symmetric and (b) the nonsymmetric stirrer configuration.

[Color figure can be viewed in the online issue, which is available at wileyonlinelibrary.com.]

depending on the piston evolution as a function of time. In general, it was observed that all particles accelerated in the *X*–*Y* direction at the same time steps which is consistent with the piston being manually driven to produce changes in the acceleration. For the stirrer configuration, a full description of the 3D particle acceleration patterns observed was beyond the scope of this work, especially given the complexity of the particles acceleration behavior depending on their position with respect to the stirrer which creates a very chaotic acceleration 3D plot. Nevertheless individual particle Lagrangian acceleration will be described in the following to illustrate the main characteristics of 3D-PTV when applied to mixing in a stir tank but without getting into the particular features of this custom-made stirred tank.

The ability to individually track, in an observation volume, a large number of particles, such as those illustrated in

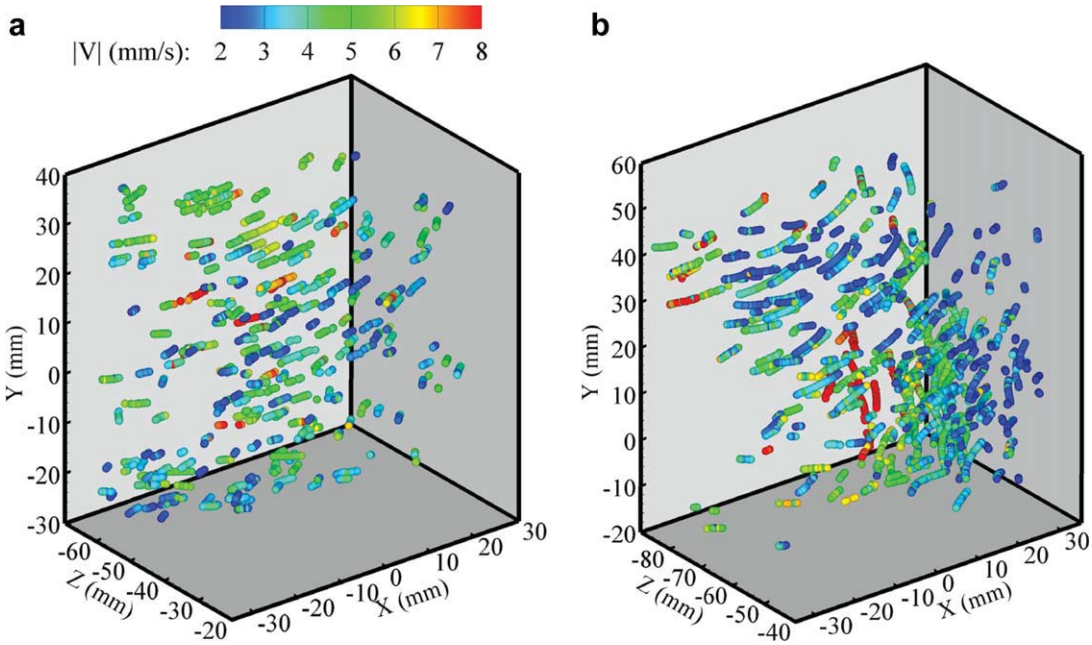

Figure 11. 3D plot of the particle velocities in the observation volume for the flows generated by (a) the symmetric and (b) the nonsymmetric stirrer configuration.

[Color figure can be viewed in the online issue, which is available at wileyonlinelibrary.com.]

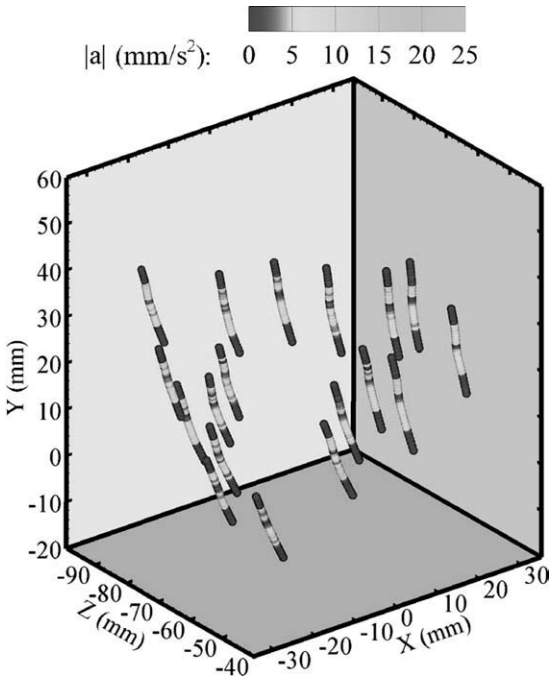

Figure 12. 3D plot of the particle accelerations in the observation volume for the quasi 1-D piston driven flow.

Figure 10, is perhaps the greatest advantage of the 3D-PTV technique over other measurement systems. The observed particle trajectories can then be classified according to their path shape, the stirrer conditions (speed, type, or position as a function of time), their position in the tank, or any other variable important to the mixing application. For example, using the present setup, with the stirrer positioned off-center in the Z direction ($X_{stir} = 0$ mm, $Z_{stir} = -115$ mm) in a rectangular tank (300 mm $\times$ 150 mm), three types of trajectories were identified in Figure 13a that did not seem to follow the circular pattern described by this stirred-driven flow. A close-up of the types of trajectories observed is illustrated in Figures 13b–d. In the general, the three trajectories show that the particles move first towards the stirrer (Z decreases) as they are drawn toward the wake of the stirrer when it moves away. Later, when the stirrer moves toward them, the particles get pushed away (Z increases) as shown in the X–Z plane in Figure 13b. This phenomenon is produced by the rectangular shape of the stirrer and its position with respect to the particles for this low Reynolds number flow. The velocity and Lagrangian acceleration are also shown in Figures 13c, d respectively. For instance, for the case with largest change in velocity, 1st type, the velocity first increases and then decreases. As shown with the trajectories, this is also consistent with the variation of the stirrer position in time. Finally, when comparing the X distance covered by the three trajectories, it was noticed that while for Type 1 the particle moved the farthest (X decreases) from its original position, for Type 2 and 3 the particles moved back and forth (X decreases and then increases) to almost the same location where they started. This is important as it would indicate their low probability of mixing. This individual description of the trajectories shows the potential of this technique to detect regions in the flow where particles might not be mixing by tracking their position as a function of time.

Conclusions and Discussion

The objective was to establish the capabilities that the optical 3D-PTV technique opens in the field of mixing in stirred tanks but also its current limitations. The bases for introducing this technique are that: (1) it determines velocity vectors and trajectories within a three-dimensional observation volume; (2) it provides the acceleration of the particles along their particle paths; (3) it describes the particle behavior of $\sim$400 particles from a Lagrangian perspective (not available in any other technique); (4) it has excellent spatial resolution as presented in Table 4. But for its direct application to many industrial processes of interest the present time resolution limit needs to be overcome. The results were shown for frame rates of 15 fps which is not sufficient for typical industrial applications although they are extremely valuable in the study of highly viscous laminar mixing processes such as those that might involve polymer blending and food processing.

What is needed to overcome this time resolution limitation is the use of higher frame rate cameras in the kHz range (i.e., 0.5–5 kHz at a resolution of at least 1000 $\times$ 1000 pixels) which are increasingly becoming available and at affordable budgets. One good solution of this type was very recently proposed by Kreizer et al.[37] were they discussed real-time image processing for PTV (at 500 Hz). Their work focused on reducing the data rates between camera and computer during PTV acquisition which is a limitation at high frame rates. Although they did not have a discussion on Lagrangian trajectories, or acceleration they showed velocity results in 2D and also proved they capabilities of PTV at high frame rates (with the added benefit of reduced data transfers needed). These type of frame rates would allow working at much larger Reynolds numbers (Re = 2000–20,000) than presented here which would permit the study of mixing in turbulent flows in industrial applications. In short, 3D-PTV is among the state-of-the-art techniques for 3D fluid measurements providing for the first time Lagrangian description of large number of particles ($\sim$400 in this study) within a stirred vessel. But it is also clear that the temporal resolution needs and can be resolved with high speed cameras so this technique can be used in more typical industrial systems.

The presented technique images, simultaneously from four cameras, an observation volume seeded with particles. The information from the four cameras is used to reconstruct the particles position in 3D space. The method then tracks the 3D particle position as a function of time (as such it could be considered a 4D PTV technique). This provides a Lagrangian description of the particles in the flow by resolving (as a function of time) their trajectory, their three components of the velocity, and their acceleration. The importance of optimizing the 3D-PTV system was described and the system was validated first on a well known quasi 1-D flow and then by comparing the results to a 2D-PIV system in a stirred tank.

The 3D-PTV technique showed great potential for the study of mixing in low Reynolds number stirred tanks where

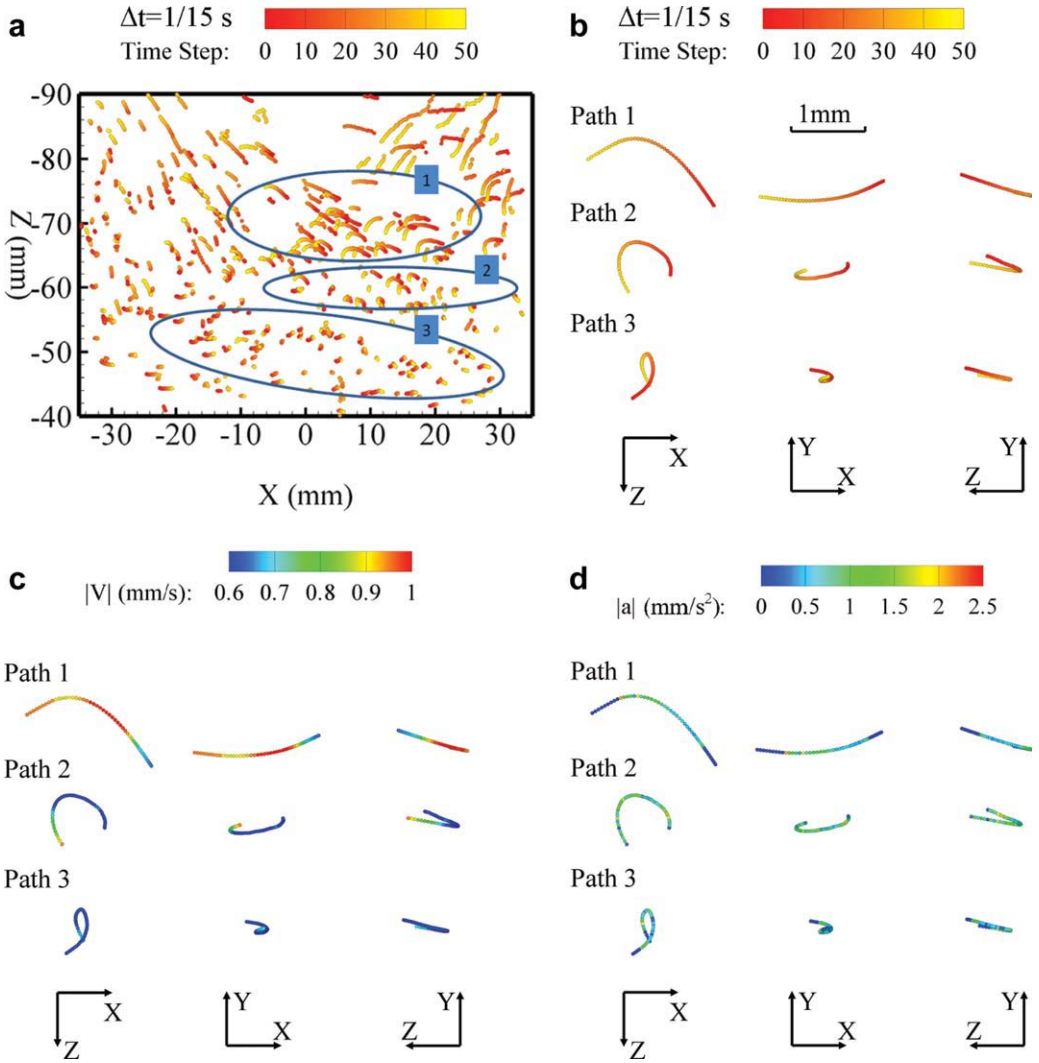

Figure 13. 3D PTV measurements showing (a) a 2D views of particle trajectories for the nonsymmetric stirrer configuration with color levels giving the time step.

A close-up shows three selected (b) particle trajectories, with (c) their velocities, and (d) their Lagrangian accelerations.

the time-resolved trajectory of particles is important to understand the dynamics of the system. For instance, the results obtained from a custom-made stirred tank described the particle trajectories for two stirrer configurations, indicating that even small changes in their configuration can produce significant changes in the particles trajectories which can result in different mixing conditions. With this technique, individual trajectories could then be extracted and classified according to their path shape and location to further understand the mixing process. Further capabilities include describing the velocity and acceleration as a function of time for individual particles.

A development area that could further enhance this technique is by using fluorescent particles and a camera filter system. Fluorescent particles have been very successful in PIV to reduce background noise and increasing the signal-to-noise ratio. This, applied to 3D-PTV, could ultimately result in the use of smaller particles. In some applications, especially those with many laser light reflections from walls of complex geometries (i.e., vessel geometry, impeller), or from other constituents of the mixture (i.e., bubbles[38] or other particles) that are not being measured, laser light reflections can be removed or highly reduced by the used of fluorescent particles (such as those containing Fluorescein or Rhodamine B). To be effective, these particles should have a good absorption at the laser wavelength and an emission wavelength sufficiently separated such that an appropriate filter in the camera will block the laser wavelength and capture the emission. Other enhancements that could be considered include increasing the depth of the observed volume or the seeding concentration, by using a scanning 3D-PTV system. Last, a 3D-PTV system could be combined with PIV for better spatial resolution or to study fluid-particle interactions.

Acknowledgments

The authors would like to acknowledge Dr. B. Lüthi, Dr. M. Holzner, and Dr. W. Kinzelbach, at ETH Zurich (Swiss Federal Institute of Technology) as well as Dr. A. Liberzon at Tel Aviv University for their support, numerous recommendations, and discussions about using their open source code for particle tracking velocimetry.

Literature Cited

1. Lamberto DJ, Muzzio FJ, Swanson PD, Tonkovich AL. Using time-dependent RPM to enhance mixing in stirred vessels. *Chem Eng Sci*. 1996;51:733–741.
2. Harvey AD, Rogers SE. Steady and unsteady computation of impeller-stirred reactors. *AIChE J*. 1996;42:2701–2712.
3. Sommerfeld M, Decker S. State of the art and future trends in CFD simulation of stirred vessel hydrodynamics. *Chem Eng Technol*. 2004;27:215–224.
4. Verzicco R, Fatica M, Iaccarino G, Orlandi P. Flow in an impeller-stirred tank using an immersed-boundary method. *AIChE J*. 2004;50: 1109–1118.
5. Sbrizzai F, Lavezzo V, Verzicco R, Campolo M, Soldati A. Direct numerical simulation of turbulent particle dispersion in an unbaffled stirred-tank reactor. *Chem Eng Sci*. 2006;61:2843–2851.
6. Arratia PE, Kukura J, Lacombe J, Muzzio FJ. Mixing of shear-thinning fluids with yield stress in stirred tanks. *AIChE J*. 2006;52: 2310–2322.
7. Mathpati CS, Deshpande SS, Joshi JB. Computational and experimental fluid dynamics of jet loop reactor. *AIChE J*. 2009;55:2526–2544.
8. Zhu HP, Zhou ZY, Yang RY, Yu AB. Discrete particle simulation of particulate systems: a review of major applications and findings. *Chem Eng Sci*. 2008;63:5728–5770.
9. Guiraud P, Costes J, Bertrand J. Local measurements of fluid and particle velocities in a stirred suspension. *Chem Eng J*. 1997;68: 75–86.
10. Yoon HS, Hill DF, Balachandar S, Adrian RJ, Ha MY. Reynolds number scaling of flow in a Rushton turbine stirred tank. Part I—mean flow, circular jet and tip vortex scaling. *Chem Eng Sci*. 2005; 60:3169–3183.
11. Lamberto DJ, Alvarez MM, Muzzio FJ. Experimental and computational investigation of the laminar flow structure in a stirred tank. *Chem Eng Sci*. 1999;54:919–942.
12. Ducci A, Yianneskis M. Vortex tracking and mixing enhancement in stirred processes. *AIChE J*. 2007;53:305–315.
13. Santos RJ, Erkoç E, Dias MM, Teixeira AM, Lopes JCB. Hydrodynamics of the mixing chamber in RIM: PIV flow-field characterization. *AIChE J*. 2008;54:1153–1163.
14. Santos RJ, Erkoç E, Dias MM, Lopes JCB. Dynamic behavior of the flow field in a RIM machine mixing chamber. *AIChE J*. 2009; 55:1338–1351.
15. Sharp KV, Hill D, Troolin D, Walters G, Lai W. Volumetric three-component velocimetry measurements of the turbulent flow around a Rushton turbine. *Exp Fluids*. 2009;48:167–183.
16. Fangary YS, Barigou M, Seville JPK, Parker DJ. Fluid trajectories in a stirred vessel of non-newtonian liquid using positron emission particle tracking. *Chem Eng Sci*. 2000;55:5969–5979.
17. Guha D, Ramachandran PA, Dudukovic MP. Flow field of suspended solids in a stirred tank reactor by Lagrangian tracking. *Chem Eng Sci*. 2007;62:6143–6154.
18. Chen J, Rados N, Al-Dahhan MH, Duduković MP, Nguyen D, Parimi K. Particle motion in packed/ebullated beds by CT and CARPT. *AIChE J*. 2001;47:994–1004.
19. Malik N, Dracos T, Papantoniou D. Particle tracking in three-dimensional turbulent flows-Part II: particle tracking. *Exp Fluids*. 1993;15: 279–294.
20. Maas HG, Gruen A. Digital photogrammetric techniques for high-resolution three-dimensional flow velocity measurements. *Opt Eng*. 1995;34:1970–1976.
21. Stüer H, Maas HG, Virant M, Becker J. A volumetric 3D measurement tool for velocity field diagnostics in microgravity experiments. *Meas Sci Technol*. 1999;10:904–913.
22. Lüthi B, Tsinober A, Kinzelbach W. Lagrangian measurement of vorticity dynamics in turbulent flow. *J Fluid Mech*. 2005;528:87–118.
23. Liberzon A, Guala M, Lüthi B, Kinzelbach W, Tsinober A. Turbulence in dilute polymer solutions. *Phys Fluids*. 2005;17:031707.
24. Nalwa VS. *A Guided Tour of Computer Vision*. Boston, MA: Addison-Wesley Longman Publishing Co., Inc., 1994.
25. Willneff J. A spatio-temporal matching algorithm for 3D particle tracking velocimetry, PhD Dissertation No. 15276, ETH, Zurich, 2003.
26. Longuet-Higgins HC. A computer algorithm for reconstructing a scene from two projections. *Nature*. 1981;293:133–135.
27. Zhang Z. Determining the epipolar geometry and its uncertainty: a review. *Int J Comput Vis*. 1998;27:161–195.
28. Hartley R, Zisserman A. *Multiple View Geometry in Computer Vision*, 2nd ed. Cambridge: Cambridge University Press, 2003.
29. Maas HG. Complexity analysis for the establishment of image correspondences of dense spatial target fields. *Int Arch Photogram Rem Sens*. 1993;29:102–102.
30. Maas HG. Complexity analysis for the establishment of image correspondences of dense spatial target fields. *Int Arch Photogramm Remote Sens*. 1992;XXIX-B5:102–107.
31. Raffel M, Willert C, Wereley S, Kompenhans J. *Particle Image Velocimetry: A Practical Guide*. New York: Springer Verlag, 2007.
32. Davies ER. *Machine Vision: Theory, Algorithms, Practicalities*, 3rd ed. San Francisco: Elsevier, 2005.
33. Papantoniou D, Maas HG. Recent advances in 3-D particle tracking velocimetry. *Proceedings 5th International Symposium on the Application of Laser Techniques in Fluid Mechanics*, Lisbon, July 1990: 9–12.
34. Sheng J, Meng H, Fox RO. Validation of CFD simulations of a stirred tank using particle image velocimetry data. *Can J Chem Eng*. 1998;76:611–625.
35. Aubin J, Le Sauze N, Bertrand J, Fletcher DF, Xuereb C. PIV measurements of flow in an aerated tank stirred by a down-and an up-pumping axial flow impeller. *Exp Thermal Fluid Sci*. 2004;28:447–456.
36. Gabriele A, Nienow AW, Simmons MJH. Use of angle resolved PIV to estimate local specific energy dissipation rates for up-and down-pumping pitched blade agitators in a stirred tank. *Chem Eng Sci*. 2009;64:126–143.
37. Kreizer M, Ratner D, Liberzon A. Real-time image processing for particle tracking velocimetry. *Exp Fluids*. 2010;48:105–110.
38. Aubin J, Le Sauze N, Bertrand J, Fletcher DF, Xuereb C. PIV measurements of flow in an aerated tank stirred by a down-and an up-pumping axial flow impeller. *Exp Thermal Fluid Sci*. 2004;28:447–456.

Manuscript received Mar. 17, 2010, and revision received Aug. 26, 2010.